Chapter 6

CuO/C Catalyzed Decarboxylative Alkenylation of Cyclic Ethers

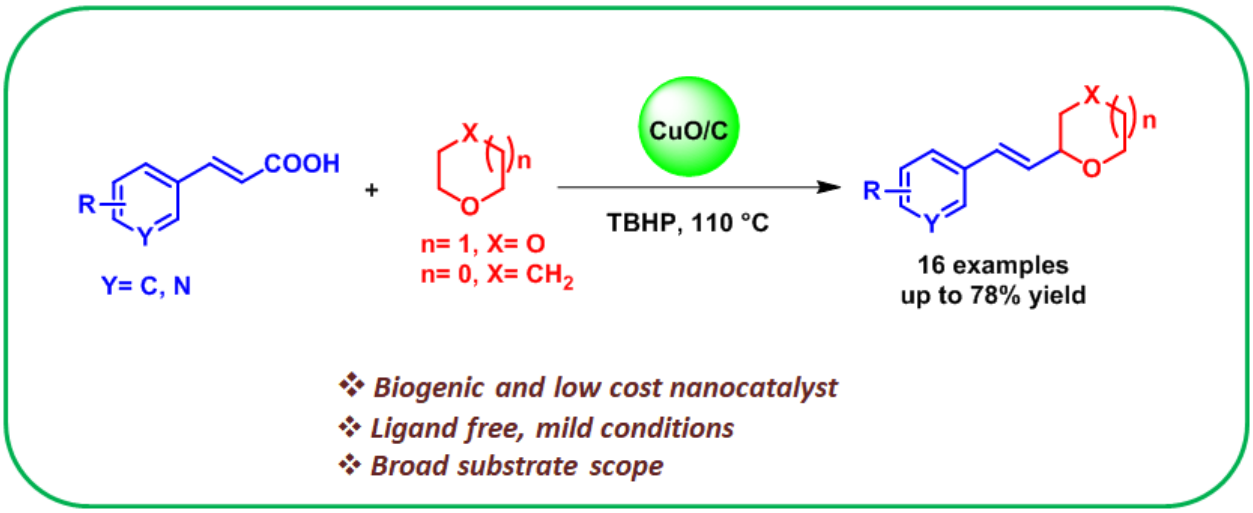

Abstract: This chapter discusses the direct C-H bond functionalization of cyclic ethers through decarboxylation by using electronically diverse cinnamic acid derivatives in presence of synthesized biogenic CuO/C nanocatalyst under mild conditions. The spherical CuO nanoparticles are prepared by hydrothermal method without using any external mediator. This methodology is suitable for electronically diverse substrates with good yields of alkenylated products. The synthesized catalyst is characterized by p-XRD, SEM-EDX, TEM, and XPS analyses. The catalyst is reusable for up to four cycles without significant loss of its catalytic activity.

6.1 Introduction

Among different types of carboxylic acids, the significance of cinnamic acids as a coupling partner in alkenylation has been realized in a report on Pd-catalyzed decarboxylative coupling with aryl halides [1]. The use of cinnamic acid as a coupling partner has significant advantages over traditional alkenylation concerning the high temperature and stereoselectivity (*E/Z*) of the product [2]. In this milieu, various methodologies have been developed for the decarboxylative coupling of cinnamic acid to form C−C, C−N, C−Si, C−S, C−P, and C−F bonds as well as in the construction of heterocycles [3]. The methods adopted in the literature reported the utilization of different metal catalysts such as salts of copper (Cu), iron (Fe), ruthenium (Ru), iridium (Ir), and manganese (Mn) [4]. In this context, Liu *et al.* developed a method of decarboxylative coupling of cinnamic acids with cyclic ethers and alcohols using Cu as the catalyst [5]. Their methodology was found to complement with the previously reported alkenylation reactions where alkynes are used at very high temperature resulting in the formation of both *E* and *Z* isomers in the product [6]. On the other hand, Pan and co-workers apprehended that cinnamic acid can be decarboxylated by using ferric acetylacetonate [$Fe(acac)_3$] for the functionalization of cyclic ethers [7]. Fang and co-workers also developed silver carbonate (Ag_2CO_3) catalyzed methodology for decarboxylative coupling of cinnamic acids with inactivated C−H bonds [8]. Direct C−H functionalization of cyclic ethers and alcohols is still a challenging task due to their poor reactivity and this is the reason they enjoy widespread use as a solvent in organic synthesis [9]. However, it is highly prevalent in some of the biologically active compounds such as sesaminone, (-)-talaumidin, idazoxan, (+)-fragrancin, lignin, etc. [10]. Therefore, exploration and development of simple and sustainable methodologies for functionalization of cyclic ethers and alcohols are highly desirable.

In the recent past, the use of different NPs in organic synthesis has received considerable interest due to their high surface to volume ratio which increases the effectiveness of the catalysts compared to the conventional ones. Biogenic NPs, in particular, have emerged as suitable alternative to the conventionally derived ones [11]. The use of carbonaceous material supports such as activated carbon [12], carbon nanotubes (CNTs) [13], reduced graphene oxides (rGO) [14], carbon quantum dots [15], graphene [16], cellulose [17], and mesoporous carbon vesicles (MCVs) [18] can enhance the catalytic activity of Cu NPs. The support material increases the stability of Cu NPs by altering their sensitivity to

oxygen, water, and other chemical entities present in the reaction mixture [19]. Li and Huang demonstrated the use of carbon layered Cu NPs in photocatalytic reduction of CO_2 [20]. The carbon layer acted as an electron transfer medium and thereby increasing the catalytic activity of the Cu NPs towards CO_2 reduction. Moreover, carbon layers such as graphene and rGO promotes interfacial contact and adhesion to the catalyst layer (CL) and thereby enhancing the ease of electron transfer or proton exchange in the reaction medium [21]. Therefore, incorporation of carbon as layers over the catalyst is warranted. Lately, the use of biomass for graphene or rGO like CL synthesis has gained attention as a green alternative due to its carbon rich and renewable nature [22]. Chen and co-workers demonstrated the use of coconut shells as a carbon source for the synthesis of graphene like bio CLs in presence of K_2CO_3 at 900 ^oC [23]. The metals such as iron can also catalyze the graphitization of amorphous carbon [24]. Our interest on biogenic NPs catalyzed organic transformations and lack of literature report on its application in decarboxylative coupling reaction compelled us to explore the prospect of bio-derived nanocatalyst in decarboxylative coupling reactions. Therefore, in this chapter we have reported the preparation of spherical copper oxide (CuO) NPs using orange peels by hydrothermal method without applying any external agents. The NPs were characterized using different spectroscopic and morphological techniques. Further, the prepared CuO NPs were employed as a catalyst in direct decarboxylative C−H functionalization of cyclic ethers and the results are reported in this chapter.

6.2 Experimental Section

6.2.1 Catalyst preparation

10 g of grounded mass of waste orange peel residue was mixed with 100 mL of distilled water. The extract was filtered through a sintered crucible and centrifuged to remove suspended particles present in the solution. In a 100 mL teflon-lined stainless steel autoclave, 4 mmol (0.79 g) of $Cu(OAc)_2.H_2O$ was dissolved in 25 mL of the aqueous extract. The solution thus obtained was stirred at room temperature until it became a homogeneous mixture. Subsequently, the homogeneous mixture was autoclaved at 195 ^oC for 7 h. The brown-coloured precipitate obtained was centrifuged and washed with water and ethanol, dried in a vacuum desiccator, and labeled as Cu/C. Further, the resulting brown-coloured mass of Cu/C was sintered at 590 ^oC for 6 h in air to get CuO/C nanocomposite.

6.2.2 General procedure for decarboxylative C-H functionalization

A 50 mL round bottomed flask equipped with a magnetic bar was charged with cinnamic acid (0.5 mmol), 1,4 dioxane (2 mL), CuO/C (10 wt%), and TBHP (3 equiv.). The reaction mixture was heated at 110 ^{o}C till the completion (monitoring by TLC) of the reaction. After completion, it was diluted with ethyl acetate and washed with distilled water. The combined organic layer was washed with brine, dried over anhydrous sodium sulfate, and concentrated under reduced pressure. The crude mixture was purified by column chromatography to afford the desired product.

6.3 Results and Discussion

6.3.1 Catalyst characterization

In a very recent report by Shi and co-workers, graphene wrapped copper catalyst was found to be shown superior catalytic properties than carbon supported ones [25]. To incorporate graphene-like layering over copper particles, carbonization of the biomass and copper was achieved at 195 ^{o}C. The resultant carbonized mass of Cu/C obtained was analyzed by p-XRD. The three peaks at 43.4°, 50.4°, and 74° were assigned to the (111), (200), and (220) lattice planes for Cu(0), respectively. The Cu/C was used in catalytic amount (10 wt% of Cu) for the model reaction of cinnamic acids and 1,4-dioxane in presence of TBHP. As expected, under this reaction condition we did not observe any conversion of the starting materials.

With these results in hand, the Cu/C obtained was heated at an elevated temperature to generate carbon layered CuO NPs. The CuO/C was analyzed with p-XRD (Figure **6.1**), the peaks with 2θ values 32.1°, 35.2°, 38.3°, 48.6°, 53.1°, 58.1°, 61.4°, 66.1°, 67.8°, 72.3°, and 74.8° were assigned to (110), (111), (111), (202), (020), (202), (113), (311), (220), (311) and (222), respectively, lattice planes of monoclinic crystalline CuO. The dome peak in the range of 15-30° inferred the presence of rGO type of carbon in the sample [26]. The p-XRD pattern of Cu/C and CuO/C agrees well with existing reference JCPDS-01-1242 and JCPDS-89-2530, respectively.

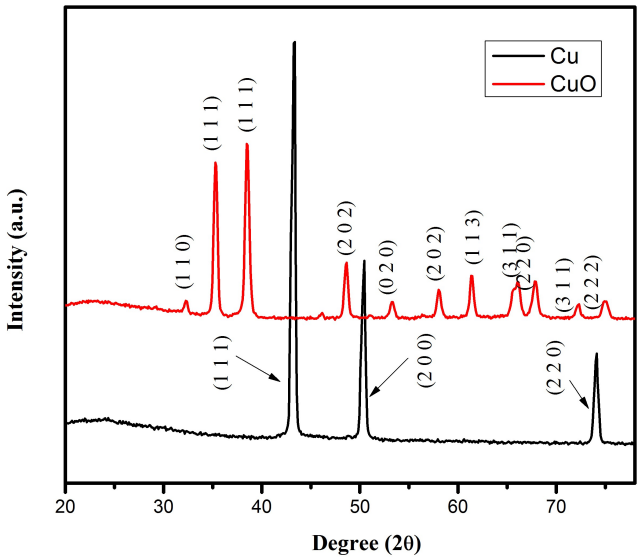

Figure **6.1**. Powder XRD pattern of Cu/C and CuO/C nanocomposites

The energy dispersive X-ray (EDX) analysis indicated the presence of Cu and O along with C and Ca (Figure **6.2**). The elements were present in the nanocomposite with an atomic percentage of carbon 21.55%, oxygen 41.45%, calcium 1.16% and copper 35.84%.

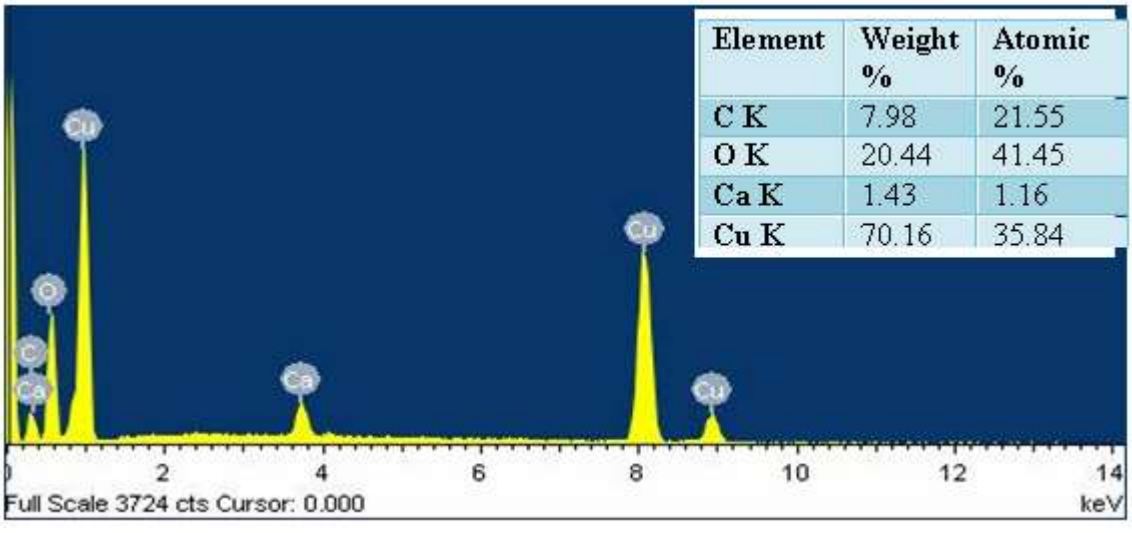

Figure **6.2**. Energy dispersive X-ray (EDX) of CuO/C nanocomposite

The surface morphology of the synthesized CuO/C was studied by SEM analysis and it showed spherical shaped nano structure formation (Figure **6.3**). Further, elemental mapping images showed the homogeneous distribution of the elements (Figure **6.4**).

TEM analysis of the synthesized CuO clearly showed a carbon layer over CuO particles (Figure **6.5a**). Interestingly, the *d* spacing (0.33 nm) obtained for carbon layer corresponds to the rGO form of carbon (Figure **6.5a**). The TEM image showed different lattice fringes for different facets associated with monoclinic CuO (Figure **6.5c**).

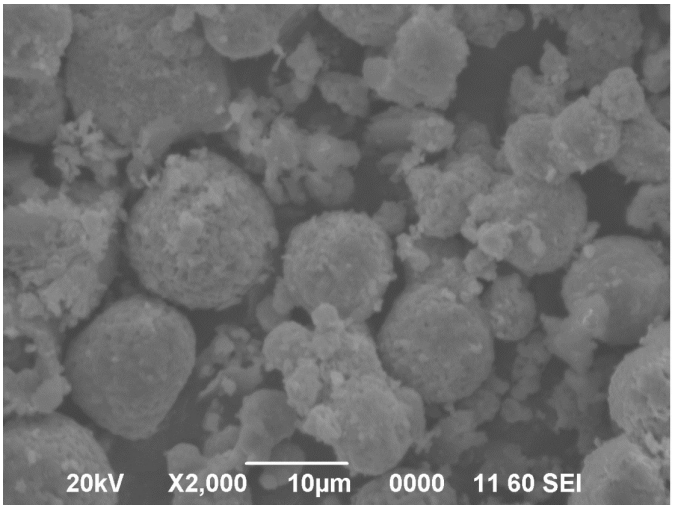

Figure **6.3**. SEM image of CuO/C nanocomposite

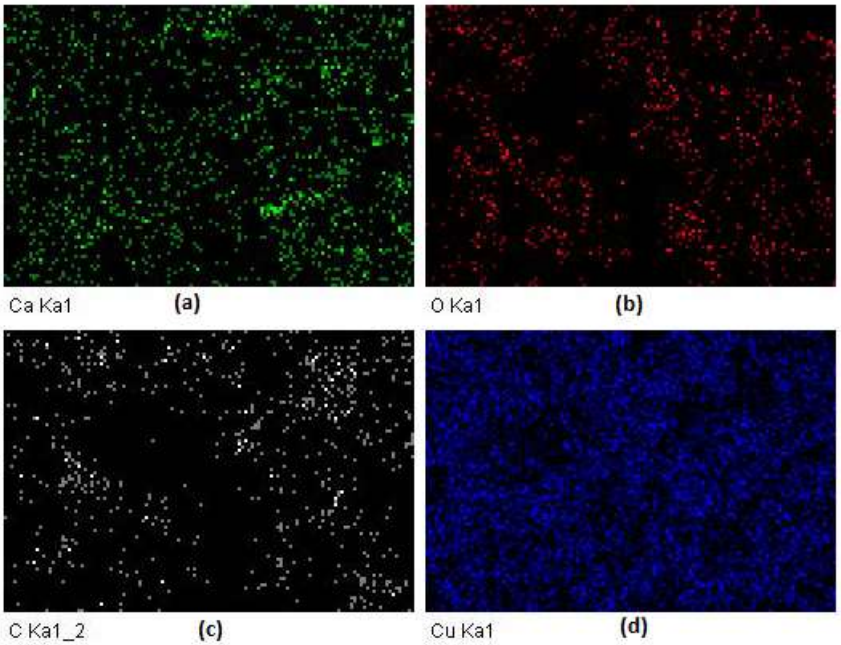

Figure **6.4**. EDS mapping images of (**a**) Ca, (**b**) O, (**c**) C, and (**d**) Cu

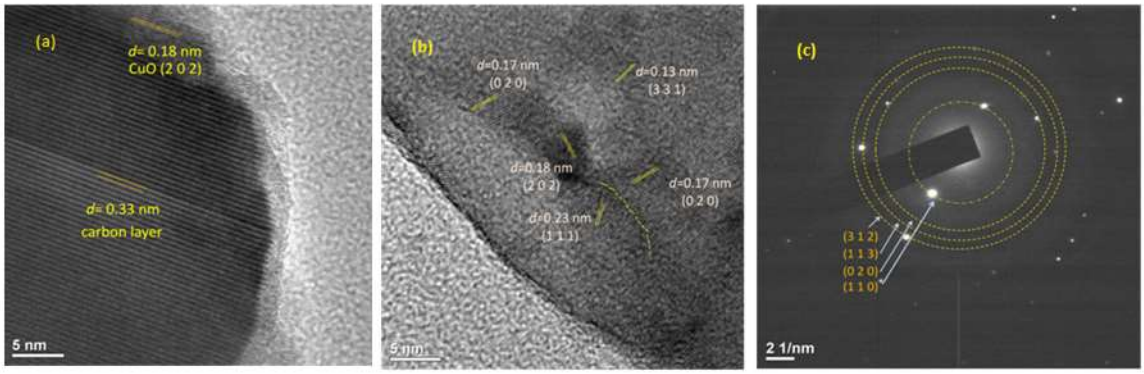

Figure **6.5**. TEM images of (**a**) Carbon layered CuO, (**b**) CuO nano, and (**c**) SAED pattern

To investigate the electronic state of the as-synthesized CuO NPs, XPS analysis was performed. The survey spectra suggested the presence of C 1s, O 1s and Cu 2p electrons in the synthesized material (Figure **6.6a**). The binding energy (B.E.) of C-C bond electrons originating from C 1s has a range of 284.6 eV to 285.2 eV. Herein, C 1s binding energy at 284.6 eV for C-C bond was taken as reference for the calibration of binding energies of other elements (Figure **6.6b**). The peak at 284.6 eV indicates the presence of sp^2 C-C type of bond in the material [27]. The shoulder peak at 288.7 eV can be attributed to O-C=O bond present in the material [28,29]. The high resolution XPS spectra for Cu 2p showed two major peaks corresponding to Cu $2p_{3/2}$ and Cu $2p_{1/2}$ at 933.93 eV and 953.62 eV, respectively (Figure **6.6d**) [30].

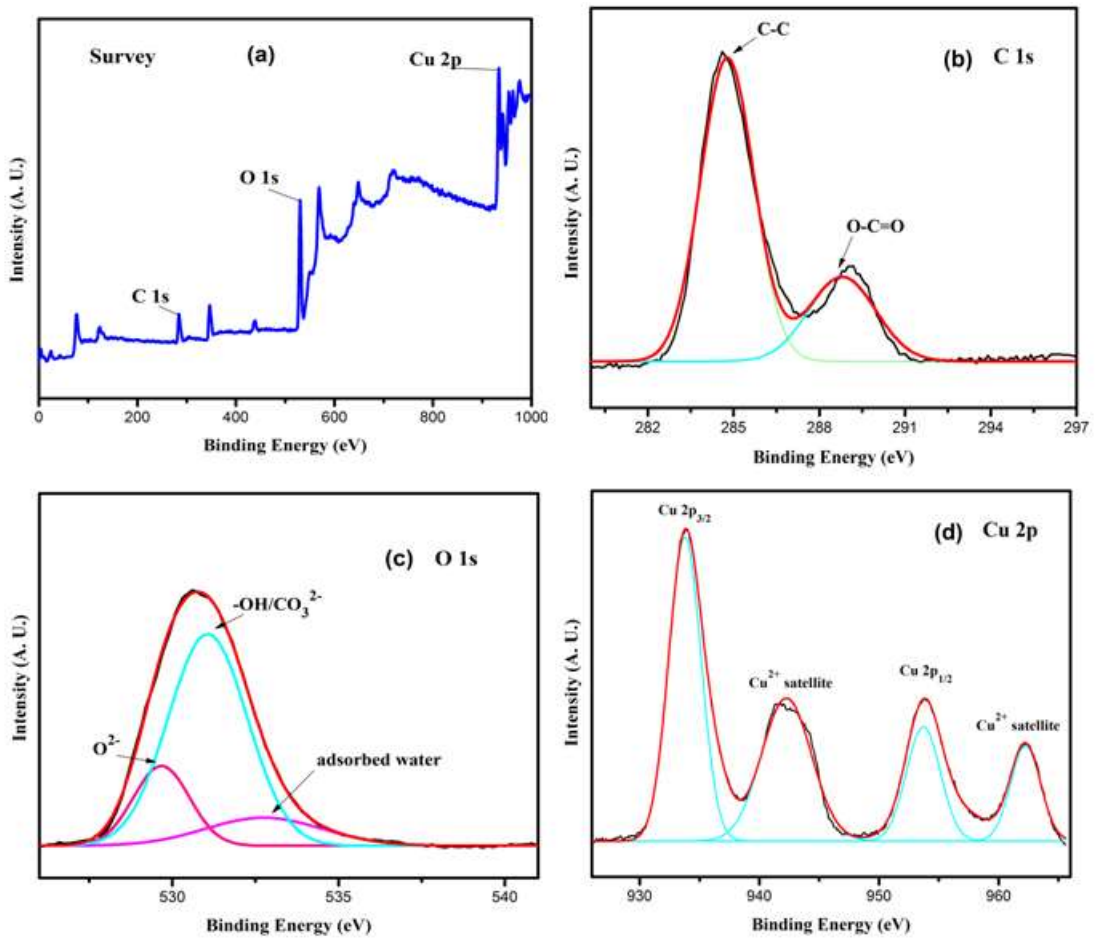

Figure **6.6**. (**a**) XPS survey scan spectrum and high resolution XPS spectra of (**b**) C 1s, (**c**) O 1s, (**d**) Cu 2p.

Further, two distinct satellite peaks approximately 9 eV higher than that of the main peaks indicated the presence of Cu^{2+} species in the sample [28,31]. The high resolution O 1s XPS spectra were deconvoluted into three peaks (Figure **6.6c**). The peak at 529.6 eV corresponds to the photoemission of O^{2-} of CuO, 531.2 eV was assigned to the emission of surface –OH and carbonate groups. From the literature, the peak at 532.8 eV was assigned to the adsorbed water on the surface of the sample [32].

6.3.2 Catalytic activity of CuO/C

6.3.2.1 Optimization of reaction conditions

We started the investigation of decarboxylative alkenylation with cinnamic acid (**1a)** and 1,4 dioxane (**2a**) as model substrates. The screening results were presented in Table **6.1**. When 10 wt% of CuO/C nanocomposite was employed in presence of 1.5 equivalent of TBHP at 100 ^{o}C, a moderate yield of the desired product was obtained (entry **1**, Table

6.1). An increase in temperature (entries **2** and **3,** Table **6.1)** had a significant impact on the reaction yield. The yield of **3a** was improved up to 74% when the 3 equivalents of TBHP was employed (entry **5**, Table **6.1**). The desired product **3a** was isolated in 66% yield in presence of 2 equivalents of TBHP (entry **7**, Table **6.1)**. A decrease in product yield was recorded with a decrease in the amount of CuO/C (entry **6**, Table **6.1)**. When we used di-*tert*-butyl peroxide (DTBP), a very less amount of product formation was observed (entry **9**, Table **6.1**). Similarly, in the oxidant-free condition the reaction furnished a trace amount of product (entry **13**, Table **6.1**). Furthermore, the reaction failed in absence of the catalyst (entry **12**, Table **6.1**), confirming that the presence of the catalyst as well as the oxidant were necessary for radical formation and decarboxylation. Other radical initiators such as H_2O_2, and $K_2S_2O_8$ could not produce the desired product. Based on these reactions the optimized reaction condition was found to be: **1a** (0.6 mmol), **2a** (2 mL), catalyst (10 wt%), and TBHP (3 equiv.) at 110 ^oC.

Table **6.1**. Optimization of the reaction conditions[a]

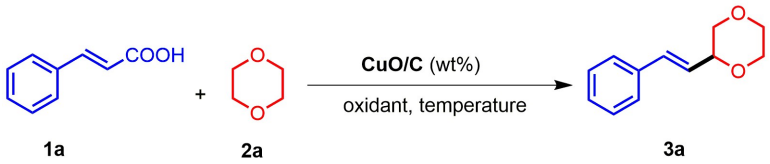

Entry	CuO/C (wt%)	Temperature (^oC)	Oxidant (equiv.)	Yield[b] (%)
1	10	100	TBHP (1.5)	46
2	10	110	TBHP (1.5)	57
3	10	120	TBHP (1.5)	58
4	10	90	TBHP (1.5)	31
5	**10**	**110**	**TBHP(3.0)**	**74**
6	5	110	TBHP (3.0)	42
7	10	110	TBHP (2.0)	66
9	10	110	DTBP (3.0)	Trace
10	10	110	H_2O_2 (3.0)	-
11	10	110	$K_2S_2O_8$ (3.0)	-
12	-	110	TBHP (3.0)	-
13	10	110	-	Trace

[a]Reaction conditions: **1a** (1 equiv.), **2a** (2 mL), for 24 h. [b]Isolated yields

6.3.2.2 Substrate scope study

With the optimized condition in hand (entry **5**, Table **6.1**), we explored the general applicability of this condition with cinnamic acids of different electronic environments. Under this reaction condition, a series of desired alkenylation products of 1,4-dioxane and THF were obtained in good yields. Among chloro-substituted cinnamic acids, *para*- (**3b**, Table **6.2**) and *meta*- (**3c**, Table **6.2**) derivatives yielded the desired product in moderate yield whereas *ortho*- (**3d**, Table **6.2**) derivatives produced an average yield of the desired product. Cinnamic acid with bromo-substituent at *para*-position also produced the desired product (**3g**, Table **6.2**) in moderate yield. Compounds containing electron-withdrawing groups reacted efficiently under this reaction condition. Substituents such as $-OCH_3$ (**3h**, Table **6.2**) and $-CH_3$ (**3e**, Table **6.2**) at *para*- position produced the alkenyl products in good yields. The *trans*-3-(3-pyridyl)acrylic acid is also a good reactant and the desired alkene (**3i**, Table **6.2**) was obtained in moderate yield. Cinnamic acids also showed a similar reactivity pattern with THF under the optimized reaction condition. Cinnamic acids having $-OCH_3$ group at *meta*- and *para*-positions along with *ortho*- and *meta*-positions resulted in good yields of alkenylated product (**3j** and **3p** respectively, Table **6.2**). Similarly, substrates containing electron-withdrawing groups (**3k** and **3m**, Table **6.2**) also carried out the reaction smoothly and furnished good to moderate yields of the desired product. In all the reactions only trans-configured (*E*) products were obtained which was confirmed by the NMR spectra.

Table **6.2**. CuO/C catalyzed decarboxylative alkenylation of cyclic ethers with cinnamic acid derivatives[a]

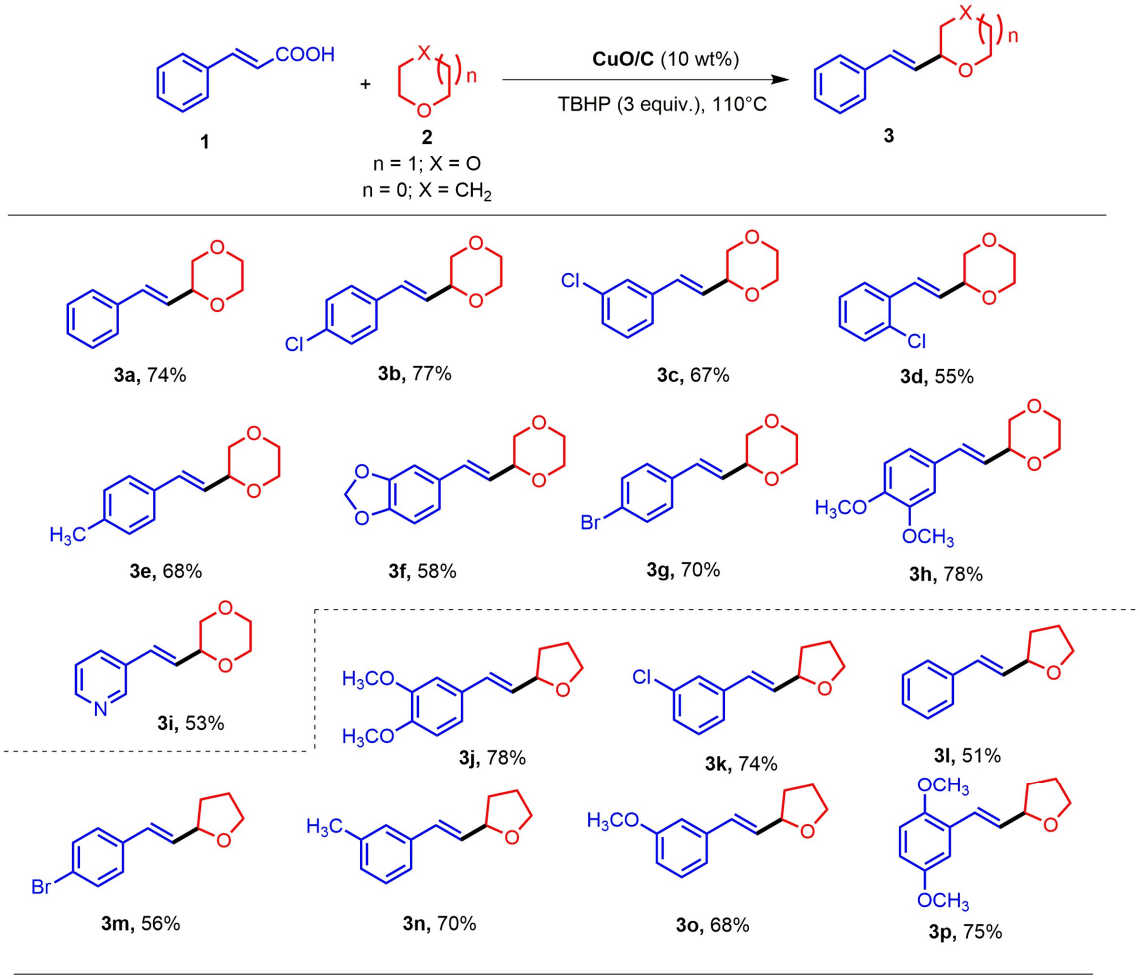

[a]Reaction conditions: **1** (1 equiv.), **2** (2mL), 24 h

6.3.2.3 Heterogeneity test

To verify the heterogeneous nature of the catalyst, a hot filtration test was done. In a round bottomed flask, CuO/C (10 wt%), TBHP (3 equiv.), and THF (2 mL) were added and stirred at 110 °C for 12 h. Then the reaction mixture was filtered and to that filtrate cinnamic acid (1 equiv.) was added. After 24 h of stirring, no product formation was observed. This suggested the heterogeneous nature of the catalyst.

6.3.2.4 Reusability test

Reusability is an important feature in heterogeneous catalysis. In our protocol, CuO/C was reusable for up to four catalytic cycles (Figure **6.7**). A little change in the reactivity of the catalyst over repeated cycles might be due to the physical loss of the catalyst. In

this test, the reaction mixture was centrifuged and then washed with ethyl acetate, and the residue obtained was dried in a vacuum desiccator. The dried catalyst was again used for the next cycle.

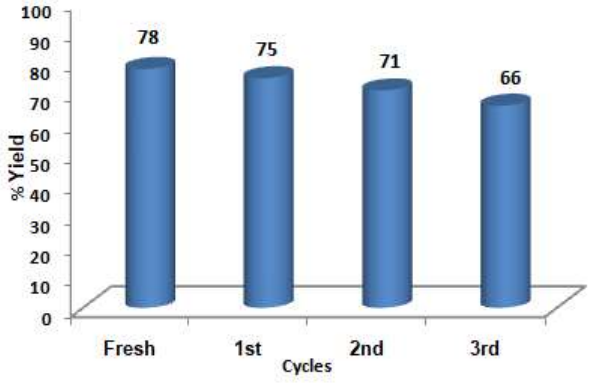

Figure **6.7**. Reusability of the catalyst over four cycles

6.3.2.5 Control experiment

Since TBHP is known as the free radical initiator, therefore it is considered that this decarboxylative functionalization proceeds through radical pathway. To investigate the possible mechanistic route, the reaction was performed in presence of a well-known radical trapping agent 2,2,6,6-tetramethylpiperidine-*N*-oxyl (TEMPO) (3 equivalents) under the optimized conditions and we observed that the reaction failed to furnished the desired product. This confirms that the current protocol follows a radical pathway.

6.3.2.6 Plausible mechanism

Based on the literature reports and experimental study, we have proposed a plausible mechanism (Scheme **6.1**) for our methodology [5,7,33]. At first, Cu(II) reacts with TBHP to form Cu(III) and *tert*-butoxy radical species in the reaction medium. This Cu(III) undergoes reduction to form Cu(II) on reaction with TBHP by releasing *t*BuOO radical and H_2O. Then *t*BuOO radical reacts with cyclic ether to generate the radical species **A**. This *t*BuOO radical along with Cu(II) forms the cupric cinnamate (**B**) by reaction with cinnamic acid. Now the reaction between cupric cinnamate and **A** finally provides the desired product **D** *via* decarboxylation and Cu(I) elimination. Oxidation of Cu(I) by *tert*-butoxy radical regenerates the cupric cinnamate that again undergoes reaction with cyclic ether.

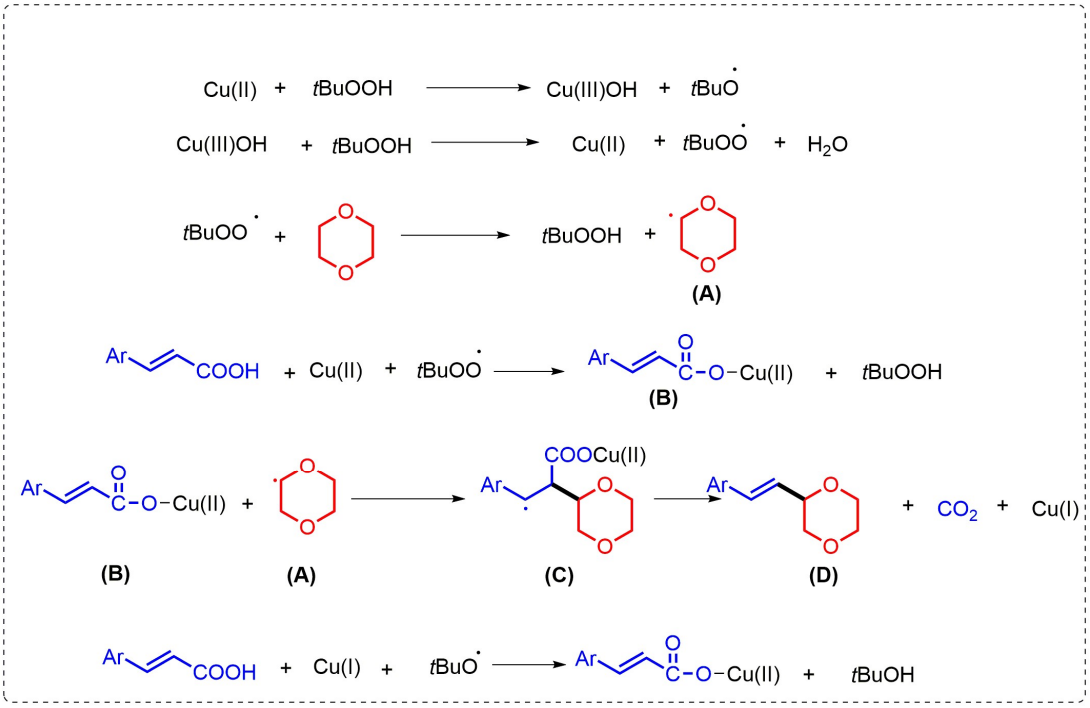

Scheme **6.1**. Possible mechanism for decarboxylative alkenylation

A comparison of the activity of the synthesized catalyst with some reported works of decarboxylative alkenylation of cyclic ethers is enlisted in Table **6.3**. From Table **6.3** it is seen that in the case of Cu and Ag-catalyzed methodologies (entries **1** and **3**, Table **6.3**) only two examples are available for the direct functionalization of cyclic ethers. Moreover, other reported works (entries **2** and **4**, Table **6.3**) are carried out either in N_2 atmosphere or in presence of a base. By comparing with these literatures, we can state that under air atmosphere we have developed a more efficient methodology for the direct decarboxylative functionalization of cyclic ethers with electronically and sterically diverse cinnamic acids in presence of easily synthesized cost-effective biogenic CuO NPs without using any additives.

Table **6.3**. Comparison of catalytic activity of reported works

Entry	Catalyst	Oxidant/Temperature(°C)/Base	Yield (%)	Reference
1	Cu	TBHP/110 (under air)	52-74 (only two examples)	5
2	$Fe(acac)_3$	DTBP/120 (under N_2)	65-81	7
3	Ag_2CO_3	DTBP/110 (under N_2)	88-89 (only two examples)	8
4	$Mn(OAc)_2.4H_2O$	TBHP/100 (under air)/DBU	25-80	34
5	CuO/C	TBHP/110 (under air)	51-78	Our work

6.4 Conclusion

In summary, we have developed a new catalytic methodology for the direct functionalization of cyclic ethers with cinnamic acid derivatives using a cheap and easily available CuO NPs. The synthesis of biogenic CuO NPs from organic waste is very easy and can be directly used in the reaction. The formation of bio-carbon layered CuO NPs is proved by different experimental techniques including, p-XRD, EDX, SEM, TEM, and XPS. The functionalization demonstrates well-tolerance towards various functional groups under ligand and base-free condition.

6.5 ^{1}H and ^{13}C NMR analytical data

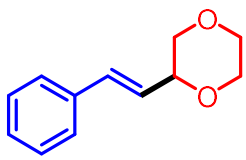

3a

(*E*)-2-styryl-1,4-dioxane (3a): ^{1}H NMR (400 MHz, $CDCl_3$): δ (ppm) 7.63–7.34 (m, 2H), 7.34–7.27 (m, 2H), 7.27–7.09 (m, 1H), 6.68 (d, J = 16.0, 1H), 6.07 (dd, J = 16.0, 6.0, 1H), 4.26–4.21 (m, 1H), 3.92–3.77 (m, 3H), 3.75–3.72 (m, 1H), 3.68−3.61 (m, 1H), 3.41 (dd, J = 11.5, 10.0, 1H); ^{13}C NMR (100 MHz, $CDCl_3$): δ (ppm) 136.64, 132.86, 128.81, 128.15, 126.71, 125.34, 76.30, 71.20, 66.82, 66.52.

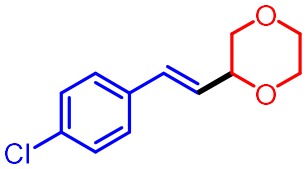

3b

(*E*)-2-(4-chlorostyryl)-1,4-dioxane (3b): ^{1}H NMR (400 MHz, $CDCl_3$): δ (ppm) 7.60–7.02 (m, 5H), 6.63 (dd, J = 16.0, 6.0, 1H), 6.04 (dd, J = 16.0, 6.0, 1H), 4.31–4.16 (m, 1H), 3.92–3.58 (m, 5H), 3.39 (dd, J = 11.0, 10.0, 1H); ^{13}C NMR (100 MHz, $CDCl_3$): δ (ppm) 134.97, 133.66, 131.46, 128.85, 127.79, 125.86, 75.97, 70.95, 66.69, 66.38.

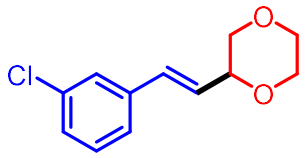

3c

(*E*)-2-(3-chlorostyryl)-1,4-dioxane (3c): ^{1}H NMR (400 MHz, $CDCl_3$): δ (ppm) 7.39–7.34 (m, 1H), 7.25–7.19 (m, 3H), 6.63 (dd, J = 16.0, 1.3, 1H), 6.09 (dd, J = 16.0, 6.0, 1H), 4.30–4.20 (m, 1H), 3.93–3.71 (m, 4H), 3.65 (m, 1H), 3.40 (dd, J = 11.5, 10.0, 1H); ^{13}C NMR (100 MHz, $CDCl_3$): δ (ppm) 138.39, 134.63, 131.21, 129.89, 127.90, 126.77, 126.46, 124.81, 75.83, 70.96, 66.67, 66.39.

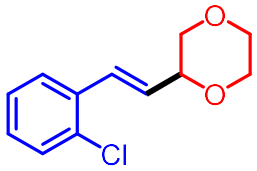

3d

(*E*)-2-(2-chlorostyryl)-1,4-dioxane (3d): ^{1}H NMR (400 MHz, $CDCl_3$): δ (ppm) 7.57–7.45 (m, 1H), 7.38–7.31 (m, 1H), 7.24–7.14 (m, 2H), 7.07 (dd, J = 16.2, 1.1, 1H), 6.07 (dd, J = 16.0, 6.2, 1H), 4.31–4.26 (m, 1H), 3.94–3.71 (m, 4H), 3.71–3.62 (m, 1H), 3.43 (dd, J = 11.5, 10.0, 1H); ^{13}C NMR (100 MHz, $CDCl_3$): δ (ppm) 134.79, 133.48, 129.95, 129.07, 129.02, 128.33, 128.23, 127.05, 76.19, 71.05, 66.78, 66.50.

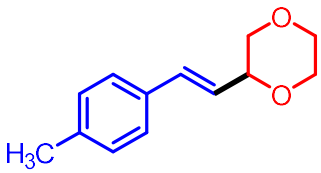

3e

(*E*)-2-(4-methylstyryl)-1,4-dioxane (3e): ^{1}H NMR (400 MHz, $CDCl_3$): δ (ppm) 7.26 (d, J = 8.4, 1H), 7.11 (d, J = 8.0, 1H), 6.65 (d, J = 16.1, 1H), 6.02 (dd, J = 16.1, 6.3, 1H), 4.29–4.18 (m, 1H), 3.79 (m, 2H), 3.65 (m, 1H), 3.41 (dd, J = 11.5, 10.0, 1H), 2.33 (s, 1H); ^{13}C NMR (100 MHz, $CDCl_3$): δ (ppm) 138.05, 133.84, 132.92, 129.51, 126.66, 124.24, 76.44, 71.24, 66.84, 66.53, 21.45.

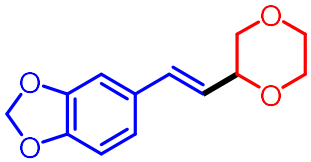

3f

(*E*)-5-(2-(1,4-dioxan-2-yl)vinyl)benzo[d][1,3]dioxole (3f): ^{1}H NMR (400 MHz, $CDCl_3$): δ (ppm) 6.91 (d, J = 1.7, 1H), 6.81 (dd, J = 8.0, 1.6, 1H), 6.74 (d, J = 8.0, 1H), 6.59 (dd, J = 16.0, 1.2, 1H), 5.95 (s, 2H), 5.90 (dd, J = 16.0, 6.3, 1H), 4.23–4.18 (m, 1H), 3.92–3.70 (m, 4H), 3.67–3.61 (m, 1H), 3.40 (dd, J = 11.5, 10.0, 1H); ^{13}C NMR (100 MHz, $CDCl_3$): δ (ppm) 148.04, 147.52, 132.46, 130.87, 123.28, 121.40, 108.28, 105.72, 101.12, 76.12, 70.99, 66.61, 66.29.

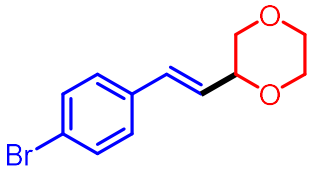

3g

(*E*)-2-(4-bromostyryl)-1,4-dioxane (3g): ^{1}H NMR (400 MHz, $CDCl_3$): δ (ppm) 7.43 (dd, J = 8.8, 2.1, 2H), 7.26–7.01 (m, 2H), 6.63 (d, J = 16.6, 1H), 6.07 (dd, J = 16.0, 6.2, 1H), 4.26–4.21 (m, 1H), 3.92–3.72 (m, 4H), 3.68–3.65 (m, 1H), 3.40 (dd, J = 11.4, 10.1, 1H); ^{13}C NMR (100 MHz, $CDCl_3$): δ (ppm) 135.55, 131.96, 131.62, 128.27, 126.10, 121.96, 76.10, 71.01, 66.83, 66.52.

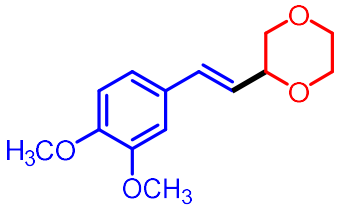

3h

(*E*)-2-(3,4-dimethoxystyryl)-1,4-dioxane (3h): ^{1}H NMR (400 MHz, $CDCl_3$): δ (ppm) 6.97–6.84 (m, 2H), 6.79 (d, J = 8.2, 1H), 6.60 (dd, J = 16.1, 0.9, 1H), 5.93 (dd, J = 16.0, 6.4, 1H), 4.34–4.11 (m, 1H), 3.87 (s, 3H), 3.85 (s, 3H), 3.84–3.75 (m, 3H), 3.75–3.69 (m, 1H), 3.66–3.60 (m, 1H), 3.41 (dd, J = 11.5, 10.0, 1H); ^{13}C NMR (100 MHz, $CDCl_3$): δ (ppm) 149.27, 149.19, 132.81, 129.62, 123.25, 120.08, 111.22, 108.93, 76.35, 71.14, 66.78, 66.47, 56.02, 55.92.

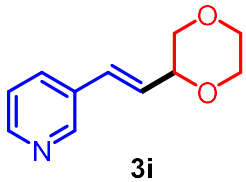

3i

(*E*)-3-(2-(1,4-dioxan-2-yl)vinyl)pyridine (3i): ^{1}H NMR (400 MHz, $CDCl_3$): δ (ppm) 8.60 (d, J = 1.6, 1H), 8.48 (dd, J = 4.8, 1.2, 1H), 7.80–7.57 (m, 1H), 7.27–7.23 (m, 1H), 6.69 (dd, J = 16.0, 0.8, 1H), 6.17 (dd, J = 16.0, 5.8, 1H), 4.30–4.25 (m, 1H), 3.88–3.73 (m, 4H), 3.69–3.65 (m, 1H), 3.41 (dd, J = 11.4, 10.0, 1H); ^{13}C NMR (100 MHz, $CDCl_3$): δ (ppm) 148.92, 148.41, 133.29, 132.26, 129.0, 127.80, 123.68, 75.90, 70.93, 66.81, 66.51.

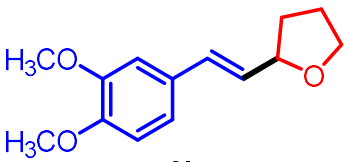

3j

(*E*)-2-(3,4-dimethoxystyryl)tetrahydrofuran (3j): ^{1}H NMR (400 MHz, $CDCl_3$): δ (ppm) 6.93–6.73 (m, 3H), 6.61–6.43 (m, 1H), 6.05 (dd, J = 15.8, 6.8 Hz, 1H), 4.43 (q, J = 7.0 Hz, 1H), 3.99–3.74 (m, 8H), 2.17–1.67 (m, 4H); ^{13}C NMR (100 Hz, $CDCl_3$): δ (ppm) 148.99, 148.77, 130.51, 129.91, 128.42, 119.82, 117.27, 111.10, 108.85, 79.96, 68.21, 55.91, 32.52, 26.06.

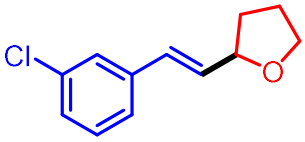

3k

(*E*)-2-(3-chlorostyryl)tetrahydrofuran (3k): ^{1}H NMR (400 MHz, $CDCl_3$): δ (ppm) 7.44–7.13 (m, 4H), 6.57–6.47 (m, 1H), 6.34–6.10 (m, 1H), 4.46 (m, 1H), 4.03–3.75 (m, 2H), 2.21–1.63 (m, 4H); ^{13}C NMR (100 Hz, $CDCl_3$): δ (ppm) 138.87, 134.53, 132.32, 130.15, 129.27, 127.48, 126.57, 124.81, 79.44, 68.33, 32.42, 25.96.

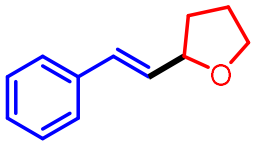

3l

(*E*)-2-styryltetrahydrofuran (3l): ^{1}H NMR (400 MHz, $CDCl_3$): δ (ppm) 7.40–7.34 (m, 2H), 7.34–7.26 (m, 2H), 7.23–7.18 (m, 1H), 6.59 (t, J = 11.7 Hz, 1H), 6.26–6.15 (m, 1H), 4.46 (m, 1H), 4.01–3.92 (m, 1H), 3.82 (m, 1H), 2.20–2.06 (m, 1H), 2.05–1.87 (m, 2H), 1.78–1.66 (m, 1H); ^{13}C NMR (100 Hz, $CDCl_3$): δ (ppm) 136.96, 130.66, 130.52, 128.63, 127.56, 126.50, 79.74, 68.25, 32.47, 25.99.

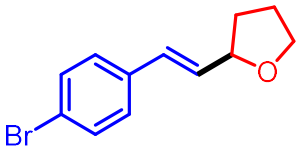

3m

(*E*)-2-(4-bromostyryl)tetrahydrofuran (3m): ^{1}H NMR (400 MHz, $CDCl_3$): δ (ppm) 7.45–7.40 (m, 2H), 7.27–7.22 (m, 2H), 6.52 (d, J = 15.9 Hz, 1H), 6.23–6.17 (m, 1H), 4.46 (q, J = 6.8 Hz, 1H), 3.99–3.82 (m, 2H), 2.17–1.60 (m, 6H); ^{13}C NMR (100 Hz, $CDCl_3$): δ (ppm) 135.84, 131.62, 131.40, 129.21, 128.00, 121.23, 79.47, 68.24, 32.34, 25.92.

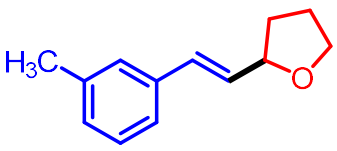

3n

(*E*)-2-(3-methylstyryl)tetrahydrofuran (3n): ^{1}H NMR (400 MHz, $CDCl_3$): δ (ppm) 7.39–6.94 (m, 4H), 6.57 (t, J = 15.4 Hz, 1H), 6.31–6.01 (m, 1H), 4.46 (q, J = 6.9 Hz, 1H), 4.09–3.75 (m, 2H), 2.33 (s, 3H), 2.24–1.63 (m, 4H); ^{13}C NMR (100 Hz, $CDCl_3$): δ (ppm) 138.12, 136.89, 130.64, 130.39, 128.53, 128.39, 127.32, 123.71, 79.95, 68.55,

32.50, 25.87, 21.91.

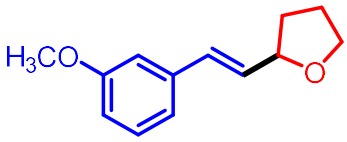

3o

(*E*)-2-(3-methoxystyryl)tetrahydrofuran (3o): ^{1}H NMR (400 MHz, $CDCl_3$): δ (ppm) 7.28–6.73 (m, 4H), 6.54 (d, J = 15.8 Hz, 1H), 6.18 (m, 1H), 4.46 (m, 1H), 4.01–3.80 (m, 2H), 3.80–3.76 (m, 3H), 2.24–1.66 (m, 4H); ^{13}C NMR (100 Hz, $CDCl_3$): δ (ppm) 159.95, 138.46, 130.95, 130.94, 129.59, 119.56, 113.81, 112.12, 79.94, 68.27, 55.39, 32.91, 25.88.

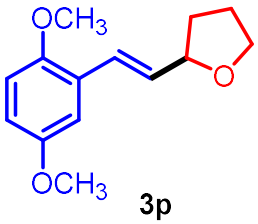

3p

(*E*)-2-(2,5-dimethoxystyryl)tetrahydrofuran (3p): ^{1}H NMR (400 MHz, $CDCl_3$): δ (ppm) 6.99 (d, J = 2.8 Hz, 1H), 6.92–6.70 (m, 3H), 6.31–6.10 (m, 1H), 4.45 (q, J = 7.1 Hz, 1H), 3.95 (m, 1H), 3.85–3.78 (m, 1H), 3.77 (s, 3H), 3.75 (s, 3H), 2.18–1.64 (m, 4H); ^{13}C NMR (100 Hz, $CDCl_3$): δ (ppm) 153.92, 151.40, 131.57, 126.83, 125.38, 113.82, 112.35, 112.14, 112.07, 80.20, 68.36, 56.27, 32.55, 25.97.

^{1}H and ^{13}C NMR spectra of (*E*)-5-(2-(1,4-dioxan-2-yl)vinyl)benzo[d][1,3]dioxole

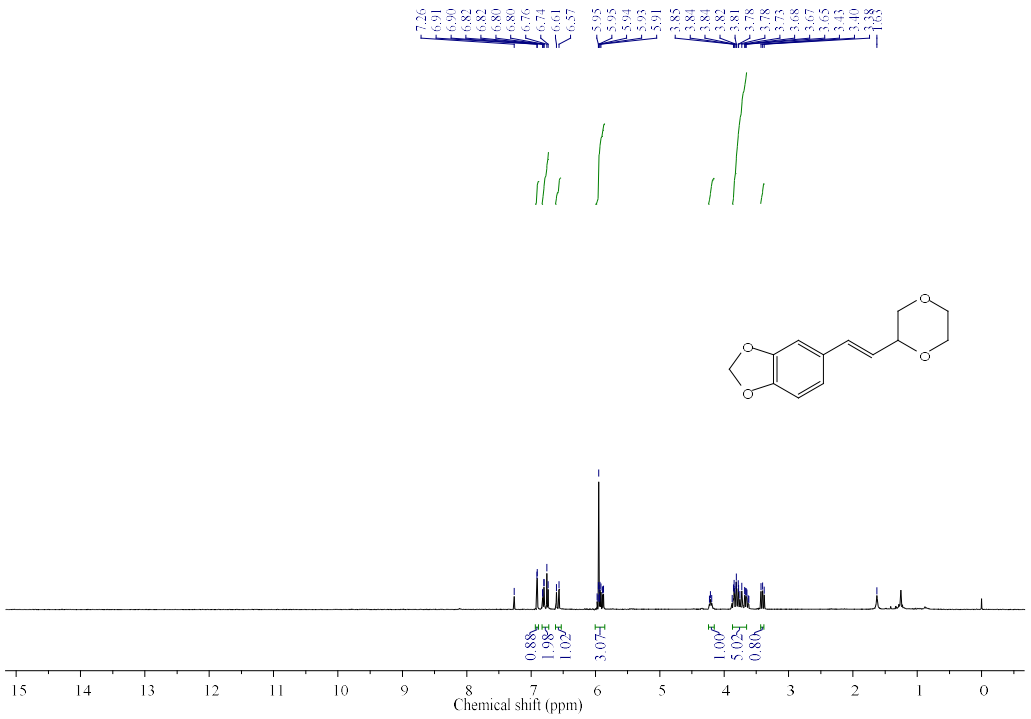

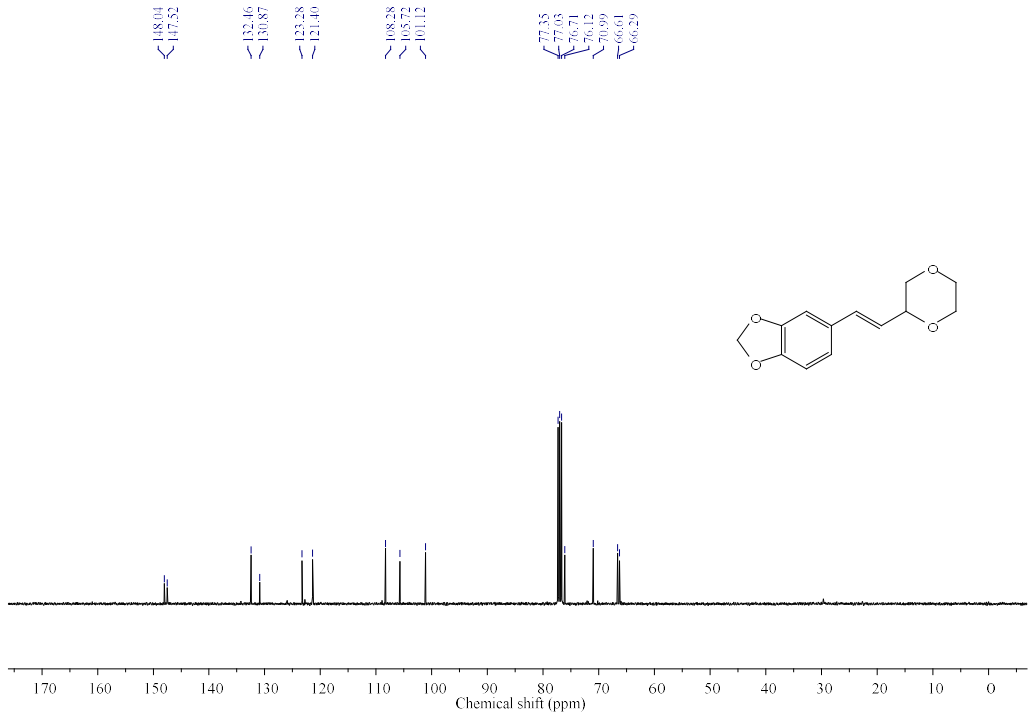

^{1}H and ^{13}C NMR spectra of (*E*)-2-(3-methoxystyryl)tetrahydrofuran

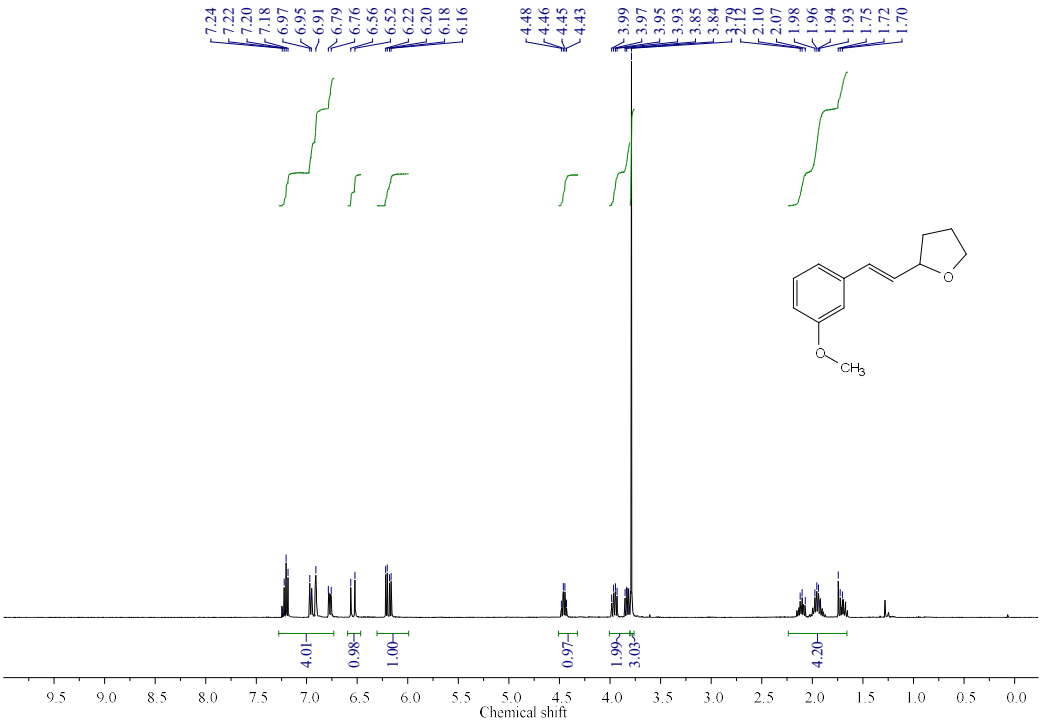

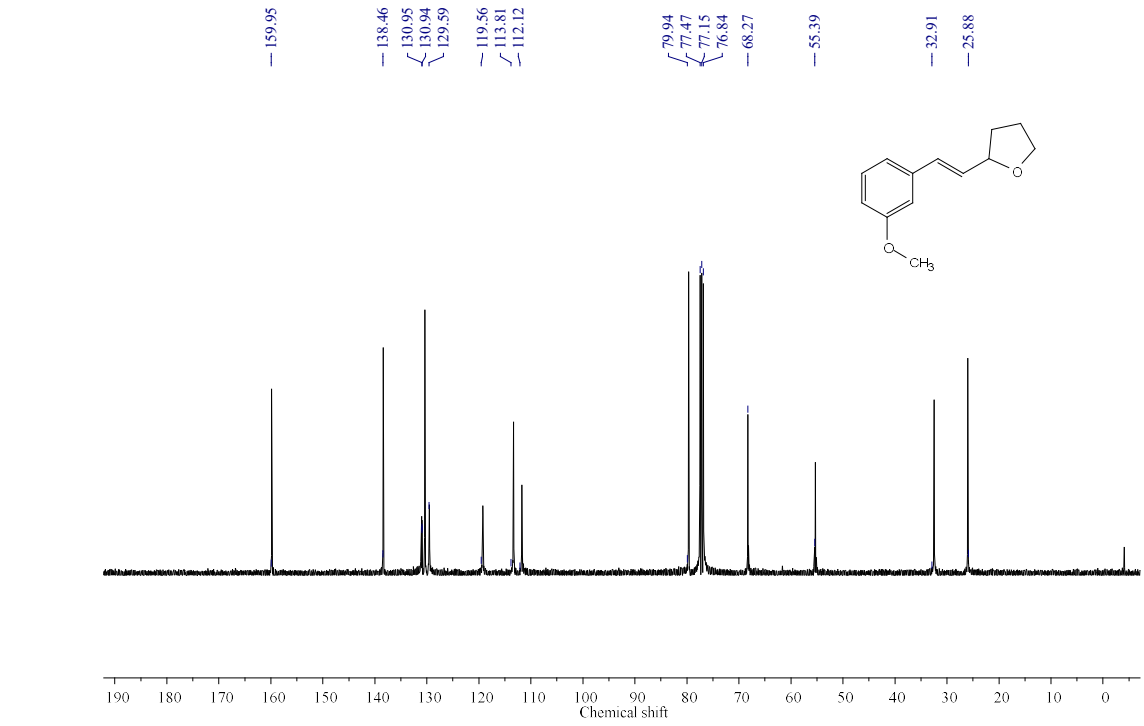

6.6 Bibliography

[1] Goossen, L. J., Rodríguez, N., Melzer, B., Linder, C., Deng, G., and Levy, L. M. Biaryl synthesis *via* Pd-catalyzed decarboxylative coupling of aromatic carboxylates with aryl halides. *Journal of the American Chemical Society*, 129(15):4824-4833, 2007.

[2] Kaur, P., Kumar, V., and Kumar, R. Recent advances in decarboxylative C-C bond formation using direct or *in situ* generated alkenyl acids. *Catalysis Reviews*, 62(1):118-161, 2020.

[3] (a) Xu, P., Abdukader, A., Hu, K., Cheng, Y., and Zhu, C. Room temperature decarboxylative trifluoromethylation of α,β-unsaturated carboxylic acids by photoredox catalysis. *Chemical Communications*, 50(18):2308-2310, 2014. (b) Zhu, X., Han, M. Y., Li, P., and Wang, L. Photoinduced difunctionalization of 2,3-dihydrofuran for the efficient synthesis of 2,3-disubstituted tetrahydrofurans. *Organic Chemistry Frontiers*, 4(8):1640-1646, 2017. (c) Govardhan, D., Bhooshan, M., Saiprakash, P. K., and Rajanna, K. C. Trichloroisocyanuric acid and $NaNO_2$ mediated nitration of indoles under acid-free and Vilsmeier-Haack conditions: synthesis and kinetic study. *SN Applied Sciences*, 1(9):1-14, 2019. (d) Natarajan, P., Chaudhary, R., and Venugopalan, P. Ipso-nitration of carboxylic acids using a mixture of nitronium tetrafluoroborate, base and 1-hexyl-3,4,5-trimethyl-1H-imidazolium tetrafluoroborate. *Tetrahedron Letters*, 60(26):1720-1723, 2019. (e) Zhang, L., Hang, Z., and Liu, Z. Q. A Free-Radical-Promoted Stereospecific Decarboxylative Silylation of α,β-Unsaturated Acids with Silanes. *Angewandte Chemie International Edition*, 55(1):236-239, 2016. (f) Li, X., Wang, M., Wang, Z., and Wang, L. Synthesis of Vinyl Sulfones through Visible Light-Induced Decarboxylative Sulfonylation of Cinnamic Acids with Disulfides. *Asian Journal of Organic Chemistry*, 8(8):1426-1435, 2019. (g) Liu, L., Zhou, D., Dong, J., Zhou, Y., Yin, S. F., and Han, L. B. Transition-metal-free C-P bond formation *via* decarboxylative phosphorylation of cinnamic acids with P-(O)-H compounds. *The Journal of Organic Chemistry*, 83(7):4190-4196, 2018.

[4] (a) Patra, T. and Maiti, D. Decarboxylation as the key step in C−C bond-forming reactions. *Chemistry–A European Journal*, 23(31):7382-7401, 2017. (b) Chen, L., Zhang, L., Yan, G., and Huang, D. Recent Advances of Cinnamic Acids in Organic Synthesis. *Asian Journal of Organic Chemistry*, 9(6):842-862, 2020.

[5] Cui, Z., Shang, X., Shao, X. F., and Liu, Z. Q. Copper-catalyzed decarboxylative alkenylation of sp^3 C–H bonds with cinnamic acids *via* a radical process. *Chemical Science*, 3(9):2853-2858, 2012.

[6] (a) Thoen, K. K., Thoen, J. C., and Uckun, F. M. Reactivity of 1,4-didehydronaphthalene toward organic hydrogen atom donors. *Tetrahedron Letters*, 41(21):4019-4024, 2000. (b) Nakagawa, T., Ozaki, H., Kamitanaka, T., Takagi, H., Matsuda, T., Kitamura, T., and Harada, T. Reactions of supercritical alcohols with unsaturated hydrocarbons. *The Journal of Supercritical Fluids*, 27(3):255-261, 2003. (c) Liu, Z. Q., Sun, L., Wang, J. G., Han, J., Zhao, Y. K., and Zhou, B. Free-radical-initiated coupling reaction of alcohols and alkynes: not C−O but C−C bond formation. *Organic Letters*, 11(6):1437-1439, 2009.

[7] Zhao, J., Zhou, W., Han, J., Li, G., and Pan, Y. Iron-catalyzed alkenylation of cyclic ethers *via* decarboxylative sp^3(C)–sp^2(C) coupling. *Tetrahedron Letters*, 54(48):6507-6510, 2013.

[8] Fang, Z., Wei, C., Lin, J., Liu, Z., Wang, W., Xu, C., Wang, X., and Wang, Y. Silver-catalyzed decarboxylative C(sp^2)–C(sp^3) coupling reactions *via* a radical mechanism. *Organic & Biomolecular Chemistry*, 15(47):9974-9978, 2017.

[9] (a) Faisca Phillips, A. M., and Pombeiro, A. J. Recent Developments in Transition Metal-Catalyzed Cross-Dehydrogenative Coupling Reactions of Ethers and Thioethers. *ChemCatChem*, 10(16):3354-3383, 2018. (b) Batra, A., Singh, P., and Singh, K. N. Recent Advances in Functionalization of α-C(sp^3)–H Centres in Inactivated Ethers through Cross Dehydrogenative Coupling. *European Journal of Organic Chemistry*, 2017(26):3739-3762, 2017.

[10] Shigehisa, H., Hayashi, M., Ohkawa, H., Suzuki, T., Okayasu, H., Mukai, M., Yamazaki, A., Kawai, R., Kikuchi, H., Satoh, Y., and Fukuyama, A. Catalytic synthesis of saturated oxygen heterocycles by hydrofunctionalization of

unactivated olefins: unprotected and protected strategies. *Journal of the American Chemical Society*, 138(33):10597-10604, 2016.

[11] (a) Mughal, B., Zaidi, S. Z. J., Zhang, X., and Hassan, S. U. Biogenic nanoparticles: Synthesis, characterisation and applications. *Applied Sciences*, 11(6):2598, 2021. (b) Tamuly, C., Saikia, I., Hazarika, M., and Das, M. R. Bio-derived CuO nanocatalyst for oxidation of aldehyde: a greener approach. *RSC Advances*, 4(40):20636-20640, 2014.

[12] Zhang, G., Li, Z., Zheng, H., Fu, T., Ju, Y., and Wang, Y. Influence of the surface oxygenated groups of activated carbon on preparation of a nano Cu/AC catalyst and heterogeneous catalysis in the oxidative carbonylation of methanol. *Applied Catalysis B: Environmental*, 179:95-105, 2015.

[13] Zhao, D., Zhang, G., Yan, L., Kong, L., Zheng, H., Mi, J., and Li, Z. Carbon nanotube-supported Cu-based catalysts for oxidative carbonylation of methanol to methyl carbonate: effect of nanotube pore size. *Catalysis Science & Technology*, 10(8):2615-2626, 2020.

[14] Yang, Z., Hao, X., Chen, S., Ma, Z., Wang, W., Wang, C., Yue, L., Sun, H., Shao, Q., Murugadoss, V., and Guo, Z. Long-term antibacterial stable reduced graphene oxide nanocomposites loaded with cuprous oxide nanoparticles. *Journal of Colloid and Interface Science*, 533:13-23, 2019.

[15] Wei, G., Wang, L., Huo, L., and Zhang, Y. Economical, green and rapid synthesis of CDs-Cu_2O/CuO nanotube from the biomass waste reed as sensitive sensing platform for the electrochemical detection of hydrazine. *Talanta*, 209:120431, 2020.

[16] (a) Guo, X., Hao, C., Jin, G., Zhu, H. Y., and Guo, X. Y. Copper nanoparticles on graphene support: an efficient photocatalyst for coupling of nitroaromatics in visible light. *Angewandte Chemie International Edition*, 53(7):1973-1977, 2014. (b) Mondal, P., Sinha, A., Salam, N., Roy, A. S., Jana, N. R., and Islam, S. M. Enhanced catalytic performance by copper nanoparticle-graphene based composite. *RSC Advances*, 3(16):5615-5623, 2013.

[17] Shim, I. W., Noh, W. T., Kwon, J. W., Jo, J. Y., Kim, K. S., and Kang, D. H. Preparation of copper nanoparticles in cellulose acetate polymer and the

reaction chemistry of copper complexes in the polymer. *Bulletin of the Korean Chemical Society*, 23(4):563-566, 2002.

[18] Li, M., Bo, X., Zhang, Y., Han, C., Nsabimana, A., and Guo, L. Cobalt and nitrogen co-embedded onion-like mesoporous carbon vesicles as efficient catalysts for oxygen reduction reaction. *Journal of Materials Chemistry A*, 2(30):11672-11682, 2014.

[19] Gawande, M. B., Goswami, A., Felpin, F. X., Asefa, T., Huang, X., Silva, R., Zou, X., Zboril, R., and Varma, R. S. Cu and Cu-based nanoparticles: synthesis and applications in catalysis. *Chemical Reviews*, 116(6):3722-3811, 2016.

[20] Li, H., Deng, Y., Liu, Y., Zeng, X., Wiley, D., and Huang, J. Carbon quantum dots and carbon layer double protected cuprous oxide for efficient visible light CO_2 reduction. *Chemical Communications*, 55(30):4419-4422, 2019.

[21] Leeuwner, M. J., Patra, A., Wilkinson, D. P., and Gyenge, E. L. Graphene and reduced graphene oxide based microporous layers for high-performance proton-exchange membrane fuel cells under varied humidity operation. *Journal of Power Sources*, 423:192-202, 2019.

[22] Safian, M. T. U., Haron, U. S., and Ibrahim, M. M. A review on bio-based graphene derived from biomass wastes. *BioResources*, 15(4):9756, 2020.

[23] Xia, J., Zhang, N., Chong, S., Chen, Y., and Sun, C. Three-dimensional porous graphene-like sheets synthesized from biocarbon *via* low-temperature graphitization for a super capacitor. *Green Chemistry*, 20(3):694-700, 2018.

[24] (a) Mun, S. P., Cai, Z., and Zhang, J. Fe-catalyzed thermal conversion of sodium lignosulfonate to graphene. *Materials Letters*, 100:180-183, 2013. (b) Eizenberg, M. and Blakely, J. M. Carbon monolayer phase condensation on Ni(111). *Surface Science*, 82(1):228-236. 1979. (c) Kalita, G., Wakita, K., and Umeno, M. Monolayer graphene from a green solid precursor. *Physica E: Low-dimensional Systems and Nanostructures*, 43(8):1490-1493, 2011.

[25] Shi, R., Zhao, J., Quan, Y., Pei, Y., Wang, X., Li, Z., and Ren, J. Carbon-Supported Nitrogen-Doped Graphene-Wrapped Copper Nanoparticles: An Effective Catalyst for the Oxidative Carbonylation of Methanol. *Industrial & Engineering Chemistry Research*, 60(7):2944-2953, 2021.

[26] (a) Huang, Y., Huang, Z., Zhong, Z., Yang, X., Hong, Q., Wang, H., Huang, S., Gao, N., Chen, X., Cai, D., and Kang, J. Highly transparent light emitting diodes on graphene encapsulated Cu nanowires network. *Scientific Reports*, 8(1):1-11, 2018. (b) Hayes, W. I., Joseph, P., Mughal, M. Z., and Papakonstantinou, P. Production of reduced graphene oxide *via* hydrothermal reduction in an aqueous sulphuric acid suspension and its electrochemical behaviour. *Journal of Solid State Electrochemistry*, 19(2):361-380, 2015.

[27] Wang, Q., Hisatomi, T., Suzuki, Y., Pan, Z., Seo, J., Katayama, M., Minegishi, T., Nishiyama, H., Takata, T., Seki, K., and Kudo, A. Particulate photocatalyst sheets based on carbon conductor layer for efficient Z-scheme pure-water splitting at ambient pressure. *Journal of the American Chemical Society*, 139(4):1675-1683, 2017.

[28] Kozak, D. S., Sergiienko, R. A., Shibata, E., Iizuka, A., and Nakamura, T. Non-electrolytic synthesis of copper oxide/carbon nanocomposite by surface plasma in super-dehydrated ethanol. *Scientific Reports*, 6(1):1-9, 2016.

[29] Gopiraman, M., Babu, S. G., Khatri, Z., Kai, W., Kim, Y. A., Endo, M., Karvembu, R., and Kim, I. S. An efficient, reusable copper-oxide/carbon-nanotube catalyst for *N*-arylation of imidazole. *Carbon*, 62:135-148, 2013.

[30] Gopiraman, M., Deng, D., Ganesh Babu, S., Hayashi, T., Karvembu, R., and Kim, I. S. Sustainable and versatile CuO/GNS nanocatalyst for highly efficient base-free coupling reactions. *ACS Sustainable Chemistry & Engineering*, 3(10):2478-2488, 2015.

[31] (a) Han, W. K., Choi, J. W., Hwang, G. H., Hong, S. J., Lee, J. S., and Kang, S. G. Fabrication of Cu nanoparticles by direct electrochemical reduction from CuO nanoparticles. *Applied Surface Science*, 252(8):2832-2838, 2006. (b) Xu, L., Li, J., Sun, H., Guo, X., Xu, J., Zhang, H., and Zhang, X. *In situ* growth of Cu_2O/CuO nanosheets on Cu coating carbon cloths as a binder-free electrode for asymmetric supercapacitors. *Frontiers in Chemistry*, 7:420, 2019.

[32] Chen, Z., Kronawitter, C. X., Yang, X., Yeh, Y. W., Yao, N., and Koel, B. E. The promoting effect of tetravalent cerium on the oxygen evolution activity of copper oxide catalysts. *Physical Chemistry Chemical Physics*, 19(47):31545-31552, 2017.

[33] Khatun, N., Santra, S. K., Banerjee, A., and Patel, B. K. Nano CuO catalyzed cross dehydrogenative coupling (CDC) of aldehydes to anhydrides. *European Journal of Organic Chemistry*, 2015(6):1309-1313, 2015.

[34] Zhang, J. X., Wang, Y. J., Zhang, W., Wang, N. X., Bai, C. B., Xing, Y. L., Li, Y. H., and Wen, J. L. Selective nickel-and manganese-catalyzed decarboxylative cross-coupling of some α,β-unsaturated carboxylic acids with cyclic ethers. *Scientific Reports*, 4(1):1-5, 2014.